Concatenated Reed–Solomon/Convolutional Coding for Data Transmission in CDMA-Based Cellular Systems

Roy D. Cideciyan, *Member, IEEE,* Evangelos Eleftheriou, *Member, IEEE,* and Marcel Rupf

***Abstract*—A robust error control scheme for data transmission in CDMA-based cellular systems is proposed which employs outer Reed–Solomon codes concatenated with inner convolutional codes. The performance of this scheme is analyzed assuming nonperiodic random spreading sequences and a Rake receiver with perfect knowledge of the channel. In particular, a simple model for the memoryless inner coding channel that encompasses the effects of multiple access interference, self-noise and thermal noise is first derived. Using new tight upper bounds on bit- and symbol-error probabilities of convolutional codes over Nakagami, Rayleigh, and Rician fading multipath channels, the performance of the concatenated coding scheme is then evaluated. The Reed–Solomon/convolutional coding scheme has been adopted by the European RACE project Code Division Testbed (CODIT) and implemented in an experimental testbed. The code design methodology, which has been used to specify the 9.6-, 64-, and 128-kbit/s data traffic channels of the CODIT testbed, is presented and the single-cell CDMA capacity is computed.**

***Index Terms*— CDMA, cellular systems, concatenated coding, convolutional codes.**

I. Introduction

DS–CDMA is a modulation and multiple-access scheme based on direct-sequence spread-spectrum technology. It has been adopted in North America as a standard (IS-95) for digital cellular systems. However, the suitability of CDMA as a multiple-access technology for future mobile and personal communications systems such as the Future Public Land Mobile Telecommunication System (FPLMTS) and the Universal Mobile Telecommunication System (UMTS) pursued by various standards bodies is still under investigation. One of the main objectives of the European RACE project Code Division Testbed (CODIT) was to build an experimental testbed based on a flexible system concept that demonstrates the potential of CDMA and satisfies the requirements of future mobile and personal communications systems [1], [2].

In broad terms, the number of users a CDMA system can accommodate in an interference-limited cellular environment, i.e., the CDMA capacity, is proportional to the processing gain and the inverse of the ratio of the bit energy to the interference power spectral density E_b/I_0 [3]. Therefore, a low E_b/I_0 is instrumental for increasing the capacity of CDMA systems. The wide-band nature of CDMA allows the use of powerful low-rate codes in conjunction with spreading sequences to achieve both low E_b/I_0 and bandwidth spreading. For example, rate-1/2 and rate-1/3 convolutional codes with memory $M = 8$ (256 states) are used in IS-95 to transmit variable-rate speech in the downlink and uplink, respectively. Unlike digital voice transmission, data transmission requires a higher degree of reliability. Raw channel error rates for digital cellular transmission are typically 10^{-2} or higher, whereas future digital cellular systems require reliable data transmission with a bit-error rate of 10^{-6} or lower, depending on the application [1], [2]. Delay requirements for data, on the other hand, are less stringent than those for voice. Thus, more powerful concatenated coding schemes with large interleaving delays allowing operation at low E_b/I_0 can be used for reliable data communication.

In this paper, a concatenated coding scheme is proposed for reliable data transmission in CDMA cellular systems. This scheme employs outer Reed–Solomon (RS) codes and inner convolutional codes in conjunction with outer and inner interleavers, and can be used for both transparent and nontransparent data services [4], [5]. The use of an inner bit interleaver/deinterleaver pair renders the fading channel memoryless, and allows the convolutional code to mitigate multiuser interference more effectively. The burst errors at the output of the Viterbi decoder are randomized by the outer symbol deinterleaver, and then corrected by the symbol-error correcting outer RS code. In addition, the error-detection capability of the RS code can be used to provide a flag for automatic retransmission requests in nontransparent data services. This error control scheme has been adopted in the CODIT project for all data traffic and dedicated control channels, and has been implemented in an experimental testbed.

The performance of DS/CDMA systems with concatenated RS/convolutional coding is analyzed for nonperiodic random spreading sequences, fading multipath channels, and ideal inner/outer interleaving. In practice, nonperiodic random spreading sequences are approximated by very long pseudonoise (PN) sequences (in IS-95, PN sequences of period $2^{42} - 1$ are used). Assuming the tapped-delay-line fading multipath model and a Rake receiver [6] with perfect knowledge of the channel,

Paper approved by R. Peterson, the Editor for Spread-Spectrum Systems of the IEEE Communications Society. Manuscript received December 20, 1995; revised September 20, 1996 and April 4, 1997. This work was performed within the RACE II project CODIT (R2020) with financial contribution by the Commission of the European Community. This paper was presented in part at the IEEE GLOBECOM '96, London, U.K., November 1996.

R. D. Cideciyan and E. Eleftheriou are with the Zurich Research Laboratory, IBM Research Division, CH-8803 Rüschlikon, Switzerland.

M. Rupf is with Siemens Schweiz AG, EUK, I-34-530, 8047 Zurich, Switzerland.

Publisher Item Identifier S 0090-6778(97)07567-3.

a simple model for the memoryless inner coding channel that encompasses the effects of multiple-access interference, self-noise, and thermal noise is first derived. Unlike the usual time-limited rectangular pulse shaping as assumed, for example, in [7] and [8], our analysis is valid for time-limited as well as for band-limited pulses (widely used in practice) whose autocorrelation function satisfies the Nyquist criterion. Our approach in deriving the model for the inner coding channel is related to that in [8]. However, in addition to providing an analytical framework that includes bandwidth-efficient pulse-shaping, conditions for the uncorrelatedness of multiple-access interference on different Rake branches are obtained. Furthermore, an upper bound on the pulse-shaping coefficient, which plays an important role in determining the CDMA capacity, is obtained. It is interesting to note that this pulse-shaping coefficient is inversely proportional to a quantity known as the mitigation bandwidth [9].

The model for the memoryless inner coding channel is used to obtain new upper bounds on the bit-error and symbol-error probabilities of convolutional codes, which are tighter than the bounds in [10] and [11] and the union-Chernoff bound in [12]. These new bounds for convolutional codes are then used to obtain tight upper bounds on the codeword-error probability at the output of the RS decoder and on the bit-error probability of the concatenated RS/convolutional codes in the presence of multipath fading and multiple-access interference. The bounds derived in this paper can be adapted to the error event case and used to compute the packet error probability of DS–CDMA systems [13]–[15] in the presence of multipath fading.

Finally, the use of the performance bounds in optimizing the rate of the RS outer codes employed in the CODIT testbed is demonstrated. In particular, the design of the RS/convolutional error control scheme for the 9.6-, 64-, and 128-kbit/s data services in the CODIT system is presented, and the tradeoffs between performance and the maximum number of simultaneous users in a cell are discussed.

The paper is organized as follows. In Section II, the communications system model is introduced, and a model for the memoryless inner coding channel is derived. In Section III, new bounds on the bit-error and symbol-error probability of convolutional codes over fading multipath channels are obtained. Section IV presents the error performance analysis of the concatenated coding scheme. In Section V, the code design methodology for the data traffic channels of the CODIT project is described, and the single-cell CDMA capacity is determined. Finally, Section VI contains a brief conclusion.

II. Communications System Model

The communications model of the uplink CDMA system studied in this paper is shown in Fig. 1. The binary information sequence of the first user (reference user) is encoded by a rate $R_O = k_O/n_O$ outer $\mathrm{RS}(n_O, k_O, b)$ code defined over $\mathrm{GF}(2^b)$. The encoder maps k_O RS symbols into n_O RS symbols, where each RS symbol consists of b bits. The output of the RS encoder is outer-interleaved on a b-bit symbol basis and then encoded by a rate $R_I = k_I/n_I$ inner convolutional code with memory M, resulting in an overall code rate of $R = R_O R_I$. The enoded sequence is then BPSK-modulated at a rate of $1/T_S$, resulting in the symbol sequence $\{x_1(n)\}$, where $x_1(n) = \pm\sqrt{E_c}$ and E_c is the chip energy. This symbol sequence is then inner-interleaved and quadrature-spread by a complex sequence $\{s_1(i)\}$, where the real and imaginary parts are independent binary nonperiodic random sequences. The chip duration is T_c, the spreading factor is $g = T_s/T_c$, and $|s_q(i)|^2 = 1$ for all users $1 \leq q \leq K$. The spectrum of the chip-spaced sequence $\{\tilde{s}_1(i)\}$ is first shaped by a baseband low-pass filter $P(f)$, and then up-converted by a quadrature carrier at frequency f_0. The resulting radio signal is transmitted over a fading multipath channel in the presence of multiple-access interference and thermal noise. Fig. 1(b) shows the time-variant multipath channel seen by the first user along with the frequency up/down conversion. The transfer function of the corresponding complex equivalent baseband channel is given by

$$H(f;t) = \sum_{m=1}^{L'} h_{1m}(t) e^{-j2\pi f \tau_{1m}(t)} \tag{1}$$

where L' is the number of resolvable paths, and $h_{1m}(t)$ and $\tau_{1m}(t)$ are the complex amplitude and the delay associated with the mth path at time t, respectively. In multipath models for radio propagation, the amplitudes $|h_{1m}(t)|$ characterizing the short-term fading are mutually independent and usually Rayleigh-, Rician-, or Nakagami-distributed, whereas the phases $\arg(h_{1m}(t))$ are uniformly distributed at any time t. Furthermore, the delays of the individual paths $\tau_{1m}(t)$ usually change very slowly, and can therefore be accurately estimated and tracked by the receiver.

The received signal $r(t)$ is first filtered by the matched filter $P^*(f)$ and then demodulated by an L-branch Rake receiver $(L \leq L')$. The Rake receiver performs coherent combining, and thus has perfect knowledge of the complex channel amplitudes. The output of the Rake receiver is deinterleaved on a sample-by-sample basis, and subsequently decoded by a soft-decision Viterbi decoder. The output of the Viterbi decoder is grouped into b-bit symbols and deinterleaved on a b-bit symbol basis prior to RS decoding.

In Appendix A, it is shown that for random spreading sequences, the combination of the inner interleaver/deinterleaver pair, the quadrature spreader, the transmit/receive filter pair, the frequency up/down converter pair, the fading multipath channel, and the coherent Rake receiver can be accurately modeled by the memoryless inner coding channel shown in Fig. 2. This analysis is valid for arbitrary fading channel statistics and for time-limited pulses, as well as for band-limited pulses whose autocorrelation function satisfies the Nyquist criterion. The inner and outer codes in conjunction with the inner coding channel constitute the equivalent communications system model depicted in Fig. 2. In particular, the output of the inner coding channel is given by

$$y_1(n) = x_1(n) g \sum_{l=1}^{L} |h_{1l}|^2 \tag{2}$$

in the absence of interference. Furthermore, for an average-power controlled CDMA cellular system, we assume that the

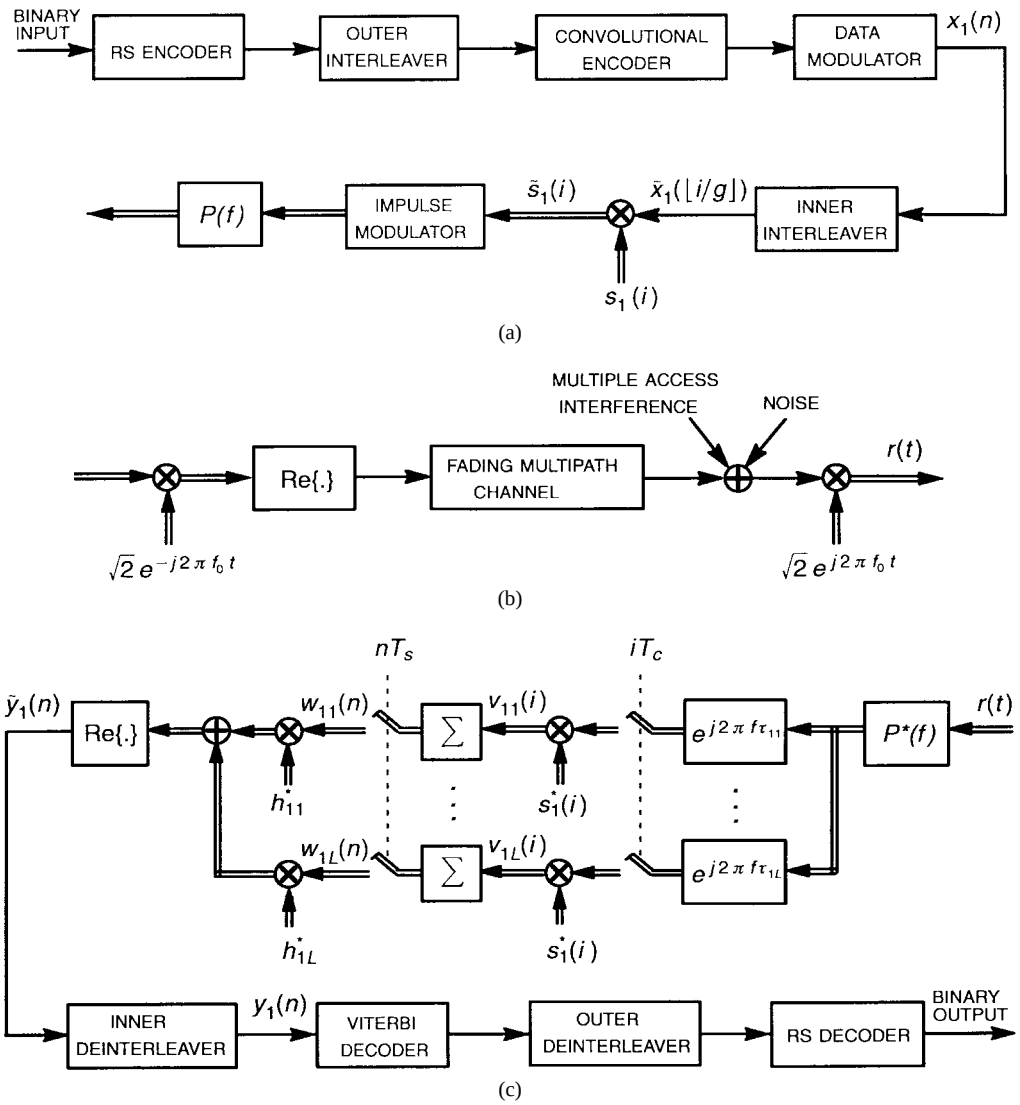

Fig. 1. Communications system model. (a) Encoder/interleaver and modulator. (b) Complex equivalent baseband channel. (c) Rake receiver and decoder/deinterleaver.

signal energy of each user received at the base station is on average equal. Consequently, for a cell with K users where the channel energy of each user is normalized to one, the variance of the total interference in (A20) can be expressed as

$$\frac{I_0}{2} = \alpha\frac{E_c}{2} + \beta(K-1)\frac{E_c}{2} + \frac{N_0}{2} \tag{3}$$

where $E_c = RE_b/g$ is the chip energy, $\alpha, 0 \le \alpha < 1$, is a parameter that depends on the second moment of the channel amplitudes [see (A14)], and $\beta, 0 < \beta \le 1$ (see Appendix B), is a parameter determined by the pulse-shaping characteristics [see (A11), (B1), and (B5)].

III. Performance Bounds for Convolutional Codes on Fading Channels

For a fading channel, the appropriate performance measure of a convolutional code, when concatenated with an RS code defined over $\mathrm{GF}(2^b)$, is the average probability $\overline{p}_s$ of a b-bit symbol at the output of the Viterbi decoder being in error. A simple bound on the average symbol-error probability $\overline{p}_s$ is

$$\overline{p}_s \le b\overline{p}_b \tag{4}$$

where $\overline{p}_b$ is the averge bit-error probability at the output of the Viterbi decoder. Using the union bound for convolutional codes [16], the average bit-error probability $\overline{p}_b$ can be computed as

$$\overline{p}_b \le \frac{1}{k_I}\sum_{d=d_f}^{\infty} a_d \overline{P}_d(\underline{x}, \underline{x}') \tag{5}$$

where a_d is the total number of nonzero information bits on all weight d trellis paths that start and end at the all-zero state, d_f is the free distance of the convolutional code, and $\overline{P}_d(\underline{x}, \underline{x}')$ is the average pairwise error probability that a correct path $\underline{x}$ differs from an incorrect path $\underline{x}'$ in d positions $i_1, i_2, \cdots, i_d$. For the equivalent communications system shown in Fig. 2, the average pairwise error probability of the first user can be

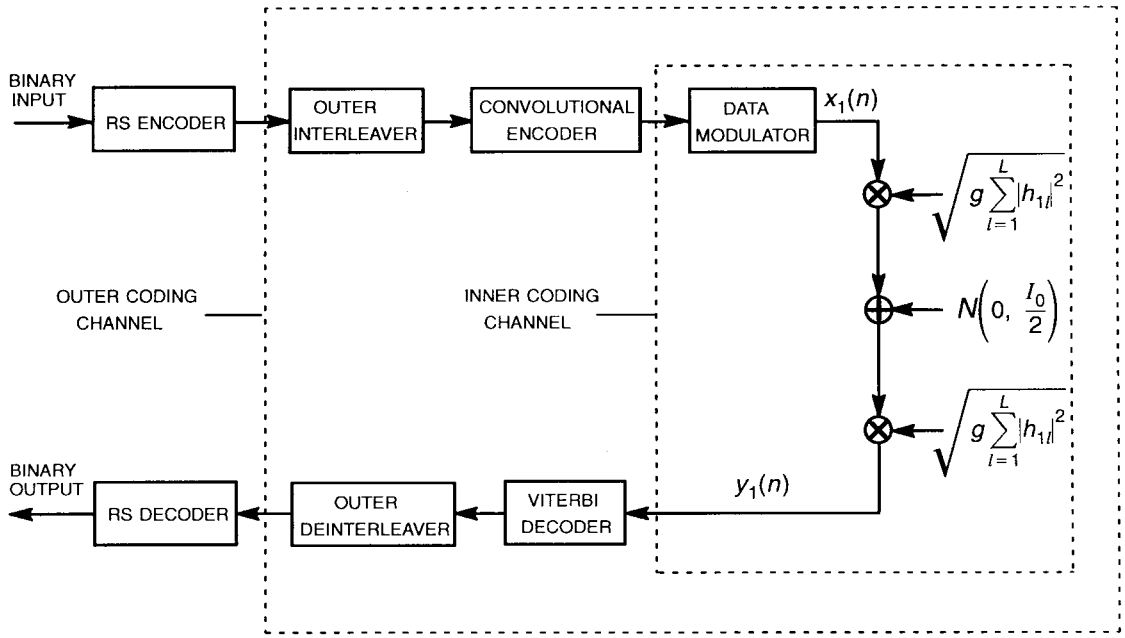

Fig. 2. Equivalent communications system model with memoryless inner coding channel.

expressed by

$$\overline{P}_d(\underline{x},\underline{x}') = \mathrm{E}\left[Q\left(\sqrt{\frac{2E_s}{I_0}\sum_{n=1}^{d}\sum_{l=1}^{L}|h_{1l}(i_n)|^2}\right)\right] \tag{6}$$

where $E_s = gE_c = RE_b$ is the symbol energy at the output of the BPSK modulator, $Q(\cdot)$ represents the tail integral of the zero-mean, unit variance normal distribution, and $\mathrm{E}[\cdot]$ denotes expectation. The expectation in (6) is taken with respect to the channel state of the first user $h_{1l}(\cdot), l = 1, 2, \cdots, L$.

Easy-to-compute, tight upper bounds on the average bit-error probability $\overline{p}_b$ of rate-k_I/n_I convolutional codes over fading multipath channels have been obtained by using the inequalities [16]

$$Q(\sqrt{x+y}) \le Q(\sqrt{x})e^{-y/2}, \qquad x \ge 0, \quad y \ge 0 \tag{7}$$

and

$$Q(\sqrt{x}) < \frac{1}{\sqrt{2\pi x}}e^{-x/2}, \qquad x > 0. \tag{8}$$

As $h_{1l}(i_n), l = 1, 2, \cdots, L, n = 1, 2, \cdots, d$, are mutually independent and $d \ge d_f$, inequalities (7) and (8) can be used to bound the average pairwise error probability as follows:

$$\overline{P}_d(\underline{x},\underline{x}') < \mathrm{E}\left[\frac{e^{-uE_s/I_0}}{\sqrt{4\pi uE_s/I_0}}\right]\mathrm{E}[e^{-vE_s/I_0}] \tag{9}$$

where the random variables u and v are defined to be

$$u = \sum_{n=1}^{d_f}\sum_{l=1}^{L}|h_{1l}(i_n)|^2, \quad v = \sum_{n=d_f+1}^{d}\sum_{l=1}^{L}|h_{1l}(i_n)|^2. \tag{10}$$

Computation of the expected values in (9) depends on the channel statistics. In the following, we shall concentrate on Nakagami and Rician fading multipath channels, of which the Rayleigh fading multipath channel is a special case.

A. Bit-Error Probability Bounds for Nakagami Fading Multipath Channels

The probability density function (pdf) of a Nakagami random variable z with mean-square value of $\Omega = \mathrm{E}[z^2]$ and an inverse normalized variance of $m = (\mathrm{E}[z^2])^2/\mathrm{var}[z^2]$ is given by [17]

$$f(z) = \frac{2m^m z^{2m-1}}{\Gamma(m)\Omega^m}e^{-(m/\Omega)z^2}, \qquad z \ge 0 \tag{11}$$

where $\Gamma(\cdot)$ is the gamma function [19]. For channel amplitudes $|h_{1l}(i_n)|, l = 1, \cdots, L$, that are independent Nakagami-distributed with parameters Ω_l and $m_l, l = 1, \cdots, L$, such that

$$\frac{m_1}{\Omega_1} = \frac{m_2}{\Omega_2} = \cdots = \frac{m_L}{\Omega_L} \tag{12}$$

it is known that both $\sqrt{u}$ and $\sqrt{v}$ are Nakagami-distributed [17]. Thus, it can be shown that u and v in (10) have the pdf of the gamma distribution given by

$$f(u) = \frac{m_T^{d_f m_T}u^{d_f m_T - 1}}{\Gamma(d_f m_T)\Omega_T^{d_f m_T}}e^{-(m_T/\Omega_T)u}, \; u \ge 0 \tag{13}$$

$$f(v) = \frac{m_T^{(d-d_f)m_T}v^{(d-d_f)m_T - 1}}{\Gamma((d-d_f)m_T)\Omega_T^{(d-d_f)m_T}}e^{-(m_T/\Omega_T)v}, \; v \ge 0 \tag{14}$$

where $m_T = \Sigma_{l=1}^{L} m_l$ and $\Omega_T = \Sigma_{l=1}^{L}\Omega_l$.

Let $A(X)$ be the generating function of the sequence $\{a_d\}, d = d_f, d_f + 1, \cdots$, i.e.,

$$A(X) = \sum_{d=d_f}^{\infty} a_d X^d = \left.\frac{\partial T(X,Y,Z)}{\partial Y}\right|_{Y=1,Z=1} \tag{15}$$

where $T(X, Y, Z)$ represents the generating function of the convolutional code [16]. Then, substituting (9) into (5) and computing the expectations with respect to the gamma pdf's

in (13) and (14), we obtain the following tight transfer function bound for the average bit-error probability

$$\overline{p}_b < \frac{1}{k_I}\frac{\Gamma(d_f m_T - 1/2)}{\Gamma(d_f m_T)}\sqrt{\frac{m_T + \Omega_T E_s/I_0}{4\pi\Omega_T E_s/I_0}}A(X_N) \quad (16)$$

where X_N is given by

$$X_N = \left(1 + \frac{\Omega_T}{m_T}\frac{E_s}{I_0}\right)^{-m_T}. \quad (17)$$

In the special case where the parameters $m_l, l = 1, \cdots, L$, are equal, we arrive at a Nakagami fading multipath channel model with equal average path strengths, i.e., $\Omega_l = 1/L', l = 1, \cdots, L$. Furthermore, when $m_l = 1, l = 1, \cdots, L$, we arrive at the widely used Rayleigh fading multipath channel model with equal average path strengths. In this case, the pdf's in (13) and (14) become central chi-square, and the bound in (16) simplifies to [18]

$$\overline{p}_b < \frac{1}{k_I}\frac{\Gamma(d_f L - 1/2)}{\Gamma(d_f L)}\sqrt{\frac{L' + E_s/I_0}{4\pi E_s/I_0}} \cdot \left.\frac{\partial T(X,Y,Z)}{\partial Y}\right|_{X=((L'+E_s/I_0)/L')^{-L}, Y=1, Z=1}. \quad (18)$$

B. Bit-Error Probability Bounds for Rician Fading Multipath Channels

The pdf of a Rician random variable z is given by

$$f(z) = \frac{z}{\sigma^2}e^{-(z^2+\mu^2)/2\sigma^2}\mathrm{I}_0\left(\frac{z\mu}{\sigma^2}\right), \qquad z \geq 0 \quad (19)$$

where $\mathrm{I}_n(\cdot)$ is the nth-order modified Bessel function of the first kind [19], μ^2 represents the mean-square value of the specular component, and $2\sigma^2$ denotes the mean-square value of the fading component. The mean-square value of z is then given by $\mathrm{E}[z^2] = 2\sigma^2 + \mu^2$. In the following, we assume that the channel amplitudes $|h_{1l}(i_n)|, l = 1, \cdots, L$, are independent Rician-distributed with arbitrary specular parameters and common fading parameters, i.e.,

$$\mu_l \geq 0 \quad \text{and} \quad \sigma_l^2 = \sigma^2, \qquad l = 1, \cdots, L. \quad (20)$$

Under these conditions, closed-form expressions for the pdf's of $\sqrt{u}$ and $\sqrt{v}$ exist [17], which can be used to show that u and v in (10) have the pdf of a noncentral chi-square distribution with $2d_f L$ and $2(d-d_f)L$ degrees of freedom and noncentrality parameter $d_f\mu_T^2$ and $(d-d_f)\mu_T^2$, respectively, i.e.,

$$f(u) = \frac{1}{2\sigma^2}\left(\frac{u}{d_f\mu_T^2}\right)^{(d_f L-1)/2} e^{-(u+d_f\mu_T^2)/2\sigma^2} \cdot \mathrm{I}_{d_f L-1}\left(\frac{\mu_T\sqrt{d_f u}}{\sigma^2}\right), \qquad u \geq 0 \quad (21)$$

$$f(v) = \frac{1}{2\sigma^2}\left(\frac{v}{(d-d_f)\mu_T^2}\right)^{((d-d_f)L-1)/2} \cdot e^{(-v+(d-d_f)\mu_T^2)/2\sigma^2}\mathrm{I}_{(d-d_f)L-1} \cdot \left(\frac{\mu_T\sqrt{(d-d_f)v}}{\sigma^2}\right), \qquad v \geq 0 \quad (22)$$

where $\mu_T^2 = \Sigma_{l=1}^{L}\mu_l^2$. Substituting (9) into (5) and computing the expectations with respect to the noncentral chi-square pdf's in (21) and (22), we obtain the following transfer function bound [20]:

$$\overline{p}_b < \frac{1}{k_I}\frac{\Gamma(d_f L - 1/2)}{\Gamma(d_f L)}{}_1F_1(1/2, d_f L, -\zeta d_f L) \cdot \sqrt{\frac{1 + 2\sigma^2 E_s/I_0}{8\pi\sigma^2 E_s/I_0}}A(X_R) \quad (23)$$

where ${}_1F_1(\cdot,\cdot,\cdot)$ denotes the confluent hypergeometric function [19],

$$\zeta = \frac{\mu_T^2}{2L\sigma^2(1 + 2\sigma^2 E_s/I_0)} \quad (24)$$

is a constant that depends on the channel statistics, and X_R is given by

$$X_R = \left(\left(1 + 2\sigma^2\frac{E_s}{I_0}\right)e^{2\sigma^2\zeta E_s/I_0}\right)^{-L}. \quad (25)$$

Note that $\mu_T^2 = 0$ results in the Rayleigh fading multipath channel model with $2\sigma^2 = 1/L'$, i.e., equal average path strengths. In this case, $\zeta = 0$ leads to ${}_1F_1(1/2, d_f L, 0) = 1$, and thus the bound in (23) simplifies to the bound in (18).

C. Symbol-Error Probability Bounds

In certain cases, tight upper bounds on the symbol-error probability at the output of the Viterbi decoder can be obtained directly from the generating function of a convolutional code. In particular, a symbol-error bound for rate-$1/n_I$ convolutional codes ($k_I = 1$) with memory M over an additive white Gaussian noise channel has been obtained in [21]. This bound can be extended to fading multipath channels by following the procedure outlined in Sections III-A and III-B. For fading channels, the average probability that a b-bit symbol at the output of the Viterbi decoder is in error is upper bounded by

$$\overline{p}_s \leq \sum_{d=d_f}^{\infty} c_d\overline{P}_d(\underline{x}, \underline{x}') \quad (26)$$

where the generating function $C(X)$ of the sequence $\{c_d\}, d = d_f, d_f + 1, \cdots,$ is given by [21]

$$C(X) = \sum_{d=d_f}^{\infty} c_d X^d = (b - 1 - M)T(X, 1, 1) + \left.\frac{\partial T(X,Y,Z)}{\partial Z}\right|_{Y=1, Z=1}. \quad (27)$$

For the Nakagami fading multipath channel models defined in Section III-A, computing the expectations in (9) using (13) and (14) and applying it to (26) leads to the transfer function bound

$$\overline{p}_s < \frac{\Gamma(d_f m_T - 1/2)}{\Gamma(d_f m_T)}\sqrt{\frac{m_T + \Omega_T E_s/I_0}{4\pi\Omega_T E_s/I_0}}C(X_N) \quad (28)$$

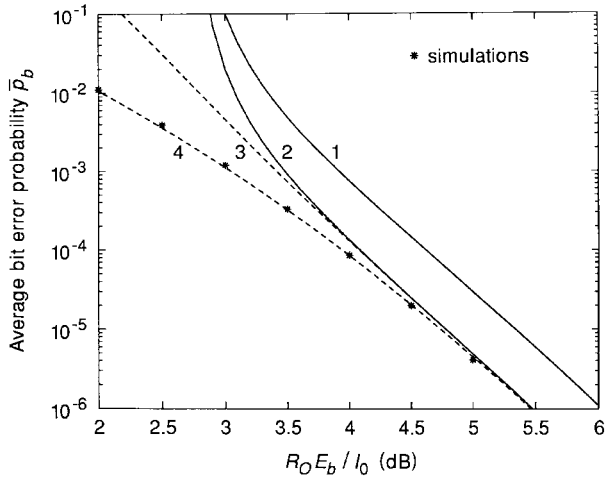

Fig. 3. Upper bounds on convolutional code performance for a Rician fading multipath $(L' = 4)$ channel.

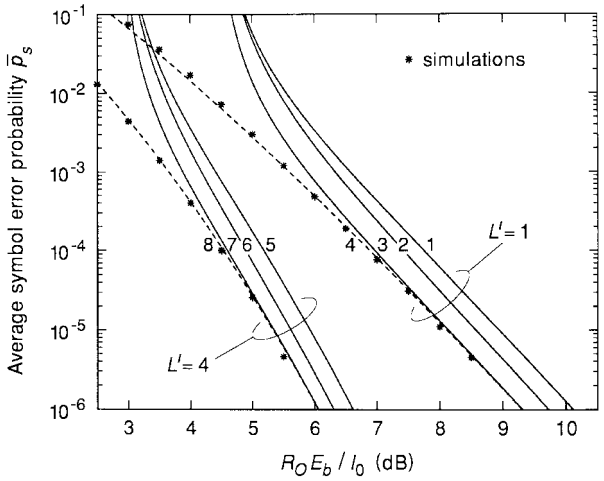

Fig. 4. Upper bounds on convolutional code performance for Rayleigh fading multipath $(L' = 1$ and $L' = 4)$ channels.

where X_N is computed according to (17). Similarly, for the Rician fading multipath channel models defined in Section III-B, averaging over the pdf's of the noncentral chi-square distribution in (21) and (22) results in the transfer function bound

$$\overline{p}_s < \frac{\Gamma(d_f L - 1/2)}{\Gamma(d_f L)} {}_1F_1(1/2, d_f L, -\zeta d_f L) \cdot \sqrt{\frac{1 + 2\sigma^2 E_s/I_0}{8\pi\sigma^2 E_s/I_0}} C(X_R) \tag{29}$$

where X_R is computed according to (25).

Although the bounds in (28) and (29) are only valid for rate-$1/n_I$ convolutional codes, it should be emphasized that this family of convolutional codes is of primary interest in DS–CDMA systems.

D. Simulation Results

Fig. 3 shows average bit-error probability bounds and simulation results as a function of $R_O E_b/I_0$ for the widely used NASA convolutional code with memory $M = 6$ (64 states) and $d_f = 10$ over a Rician fading multipath channel. In particular, $L = L' = 4$ paths with unequal average strengths were chosen where $s_1^2 = 1/4, s_2^2 = 1/8, s_3^2 = 1/16, s_4^2 = 1/16$, and $\sigma^2 = 1/16$. Curves 1 and 2 have been computed using the generating function of the NASA code in [22]. Specifically, curve 1 corresponds to the bit-error bound computed by following the approaches in [10]–[12], whereas curve 2 corresponds to the new bound in (23). Curves 3 and 4 have been computed by using the first 18 and 6 terms of the series expansion of the bound in (23), respectively. Superimposed also are simulation results demonstrating the tightness of the new bounds. It can be seen that the new bound improves on previous bounds by about 0.6 dB. Furthermore, the new bounds are particularly tight at $R_O E_b/I_0$, corresponding to $\overline{p}_b < 10^{-3}$. At low $R_O E_b/I_0$, corresponding to $10^{-3} \leq \overline{p}_b \leq 10^{-2}$, the new bounds are approximately 0.5–1 dB worse than the simulation results. Finally, we remark that the transfer function bound in (23) diverges at $R_O E_b/I_0 = 2.78$ dB, corresponding to the location of the dominant pole of the transfer function of the NASA code, i.e., $X_R = 0.41826$. Such behavior is typical for transfer-function-type union bounds. It is also interesting to observe that curve 4, which has been computed by using the first six terms of the series expansion of the bound in (23), approximates very accurately the performance of the NASA code over the entire range of $R_O E_b/I_0$.

Fig. 4 shows average symbol-error probability bounds and simulation results as a function of $R_O E_b/I_0$ for the same NASA convolutional code over a Rayleigh fading multipath channel. In particular, $L = L' = 4$ paths with equal average strengths were chosen, which is a special case of a Nakagami fading multipath channel, i.e., $m_l = 1, \Omega_l = 1/4$ for $l = 1, \cdots, 4$. In the same figure, results corresponding to a Rayleigh fading channel with a single path, i.e., $L = L' = 1$, are presented to demonstrate the diversity advantage of the Rake receiver. Curves 1, 2, 3, 5, 6, and 7 (solid lines) have been computed using the generating function of the NASA code. Specifically, curve 1 $(L = 1)$ and curve 5 $(L = 4)$ correspond to the symbol-error bound computed by following the approaches in [10]–[12], whereas curve 3 $(L = 1)$ and curve 7 $(L = 4)$ correspond to the new symbol-error bound in (28). Curve 2 $(L = 1)$ and curve 6 $(L = 4)$ have been obtained from the bit-error bound (18) in conjunction with the inequality $\overline{p}_s \leq b\overline{p}_b$. It can be seen that the new symbol-error bounds offer an improvement of about 0.8 and 0.6 dB for $L = 1$ and $L = 4$, respectively. Even the simple symbol-error bound that uses $\overline{p}_s \leq b\overline{p}_b$ offers an improvement of about 0.4 and 0.3 dB for $L = 1$ and $L = 4$, respectively. Superimposed also are simulation results demonstrating that the new bounds are particularly tight at $R_O E_b/I_0$, corresponding to $\overline{p}_b < 4 \times 10^{-3}$. Furthermore, at low $R_O E_b/I_0$, corresponding to $4 \times 10^{-3} \leq \overline{p}_b \leq 2 \times 10^{-2}$, the new bounds are approximately 0.5–1 dB worse than the simulation results. Finally, curve 4 $(L = 1)$ and curve 8 $(L = 4)$ (dashed lines) have been computed by using the first six terms of the series expansion of the symbol bound in (28). We observe that the use of the first six terms of the series expansion of the transfer function bound leads again to a very accurate approximation of the convolutional code performance over the entire range of $R_O E_b/I_0$.

IV. Performance of Concatenated Coding Scheme

An $\mathrm{RS}\,(n_O, k_O, b)$ code allows the correction of at most $\varepsilon = \lfloor (n_O - k_O)/2 \rfloor$ b-bit erroneous symbols. A bounded distance decoder raises a flag indicating decoder failure whenever it cannot find an RS codeword within a distance of $\leq \varepsilon$ of the received word. On the other hand, if a bounded distance decoder finds an RS codeword within $\leq \varepsilon$ of the received word, then there are two possible scenarios. Either the decoded word corresponds to the transmitted RS codeword (correct decoding) or the decoded word corresponds to an RS codeword other than the transmitted one (incorrect decoding).

If $\overline{p}_s$ denotes the average symbol-error rate at the input of the RS decoder (i.e., at the output of the outer deinterleaver), then the probability of codeword error P_W, which includes the contributions of both incorrect decoding and decoder failure, is given by

$$P_W = \sum_{i=\varepsilon+1}^{n_O} \binom{n_O}{i} \overline{p}_s^{\,i} (1 - \overline{p}_s)^{n_O - i}. \tag{30}$$

Because P_W decreases monotonically as $\overline{p}_s$ decreases from one to zero, the symbol-error upper bounds for convolutional codes over independent Nakagami and Rician fading multipath channels derived in Section III can be used in (30) to obtain tight upper bounds on P_W as a function of the RS/convolutional code and the parameters of the fading multipath channel.

For a systematic RS code, the probability of bit error at the output of the RS decoder can be upper bounded as follows [23]:

$$P_b < \sum_{i=\varepsilon+1}^{n_O} \frac{i+\varepsilon}{n_O} \binom{n_O}{i} \overline{p}_s^{\,i} (1 - \overline{p}_s)^{n_O - i}. \tag{31}$$

Observing again that the right-hand side of (31) decreases monotonically as $\overline{p}_s$ decreases from one to zero, the symbol-error upper bounds derived in Section III can also be used in (31) to obtain upper bounds on P_b as a function of the RS/convolutional code and the parameters of the fading channel.

In summary, the upper bounds on P_W and P_b as a function of E_b/I_0 characterize the overall error rate performance of the concatenated coding scheme over independent Nakagami and Rician fading multipath channels. Alternatively, one can use a good approximation for $\overline{p}_s$ (taking the first six terms of the series expansion of the transfer function bounds in Section III seems to be an excellent choice) in (30) and (31) to obtain an accurate estimate of P_W and P_b over the entire range of E_b/I_0.

Having studied the performance of concatened RS/convolutional coding schemes over fading multipath channels, it is interesting to demonstrate the increase of effective diversity due to coding. At high E_b/I_0, the probability of a bit error at the output of the RS decoder in (31) can be approximated by

$$P_b \approx \frac{2\varepsilon + 1}{n_O} \binom{n_O}{\varepsilon + 1} \overline{p}_s^{\,\varepsilon+1}. \tag{32}$$

Assuming now equal-strength Rayleigh or Rician fading multipath channels and an L-branch Rake receiver and using the first dominant term of the series expansion of the symbol-error bounds in (28) and (29), one can readily obtain

$$P_b \approx \xi_1 \left(1 + \frac{1}{L'} \frac{E_s}{I_0}\right)^{-L d_f (\varepsilon+1)} \tag{33}$$

for Rayleigh fading multipath channels and

$$P_b \approx \xi_2 \left(\left(1 + 2\sigma^2 \frac{E_s}{I_0}\right) e^{2\sigma^2 \zeta E_s / I_0}\right)^{-L d_f (\varepsilon+1)} \tag{34}$$

for Rician fading multipath channels, where ξ_1 and ξ_2 are constants. Expressions (33) and (34) indicate that concatenated coding increases the effective order of diversity of the overall system by a factor of $d_f(\varepsilon + 1) = d_f \lfloor (d_{\min} + 1)/2 \rfloor$, where $d_{\min}$ is the minimum distance of the RS code.

V. The CODIT System

In this section, the DS–CDMA based radio interface of CODIT, and in particular the code design for the data traffic channels, is described. The basic concept of the radio interface is illustrated in Fig. 5 [1], [2]. The following types of traffic channels (TCH) are used: a variable-rate speech traffic channel (TCH/S), data traffic channels $(\mathrm{TCH/D}x)$, where x indicates the source rate in kbit/s, and a dedicated control channel (DCCH). The concatenated RS/convolutional coding scheme discussed in the previous sections is used to encode the information bits on DCCH and $\mathrm{TCH/D}x$, whereas punctured convolutional codes are used to provide unequal error protection of the information bits on TCH/S. The radio resource manager selects the chip rate and the carrier frequency for each connection based on the requirements of the requested service, the actual traffic load, the cell characteristics, and the equipment constraints. From this information, the configuration unit then derives the parameters of all of the signal processing blocks. The physical data channel (PDCH) that arises by multiplexing the various traffic channels is based on a 10-ms frame size. In CODIT, the content of the PDCH is coherently demodulated both on the downlink and uplink. This is achieved by estimating the channel from a pilot channel in the downlink and from a training sequence derived from the auxiliary physical control channel (PCCH) in the uplink. In general, the PCCH contains information concerning the spreading factor, which varies from frame to frame, and power control (only downlink). The demodulation of the PCCH is coherent on the downlink and differentially coherent on the uplink. Binary PSK with quadrature spreading is used for both PDCH and PCCH on the downlink, whereas binary PSK and binary differential PSK in combination with offset quadrature spreading are used for PDCH and PCCH on the uplink, respectively. Two chip rates have been specified for the testbed, i.e., $1/T_c = 1.023$ and 5.115 Mchip/s, corresponding to narrow-band (NB) and medium-band (MB) CDMA transmission. Furthermore, the various spreading sequences are different phases of a very long PN sequence with period $2^{41} - 1$. Finally, square-root raised-cosine pulse-shaping filters having a rolloff parameter of $\varrho = 0.35$ are used prior to frequency up-conversion with a carrier

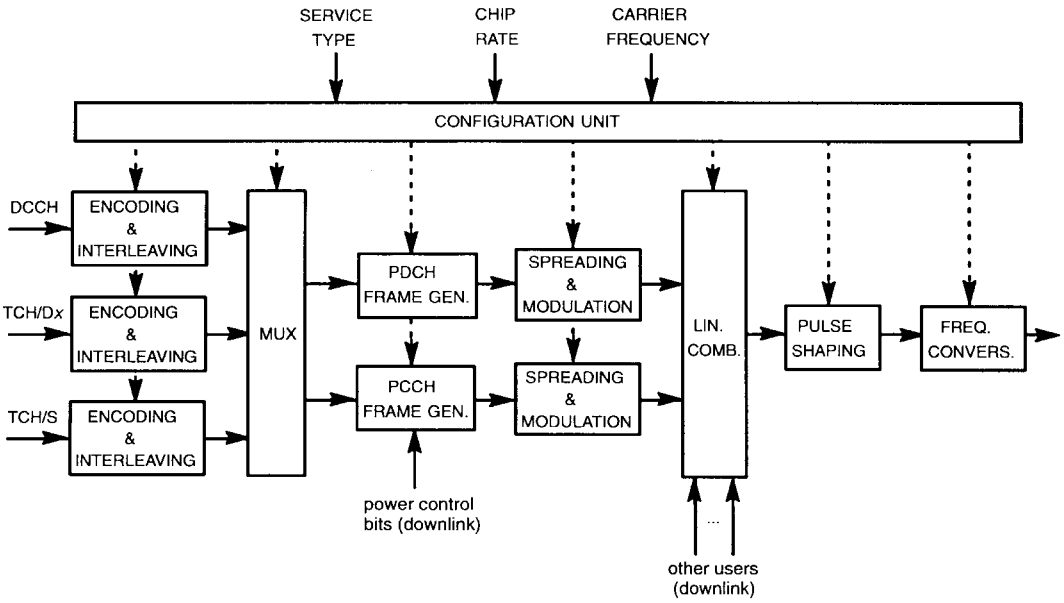

Fig. 5. CODIT transmission scheme.

at frequency $f_0 = 2.232$ GHz (uplink) or to $f_0 = 2.332$ GHz (downlink). In the receiver, after frequency down-conversion and matched filtering, the baseband signal is sampled and fed into a four-branch $(L = 4)$ coherent Rake receiver. Soft-output Viterbi decoding is used for speech, whereas soft-decision Viterbi decoding along with errors—only RS decoding is employed to recover data and control bits.

In the following, we shall concentrate on the code design for the data traffic channels TCH/Dx of the CODIT testbed where $x = 9.6$, 64, and 128 kbit/s. TCH/D9.6 has been specified for both NB and MB transmission, whereas TCH/D64 and TCH/D128 have been specified only for MB transmission. The design constraints included a total interleaving delay of at most 120 ms for data services and a bit-error rate P_b of at most 10^{-6}.

For coherent Rake reception in a fading multipath environment, the use of convolutional codes with rates $R_I < 1/4$ results in diminishing returns. Furthermore, practical synchronization circuits require a reasonably high E_s/I_0 for satisfactory operation, resulting in a lower limit on R_I. The rate of the inner convolutional code for all uplink and downlink TCH/Dx has therefore been selected to be $R_I = 1/2$. In particular, the standard $M = 6$ rate-1/2 NASA code has been chosen for the testbed. The size of the inner interleaver was selected such that for vehicle speeds greater than 25 km/h, performance of the convolutional code approaches the performance with ideal interleaving. This design strategy clearly aims at optimizing code performance at medium to high speeds, at which system performance usually is worst. At very low speeds, fast power control (closed-loop power control) and antenna diversity mitigate the performance degradation due to long deep fades. As this paper focuses on code design aspects, the effects of the fast power control on the overall system performance have not been studied.

Fig. 6 shows the average bit-error probability $\overline{p}_b$ at the output of the Viterbi decoder as a function of $R_O E_b/I_0$ for

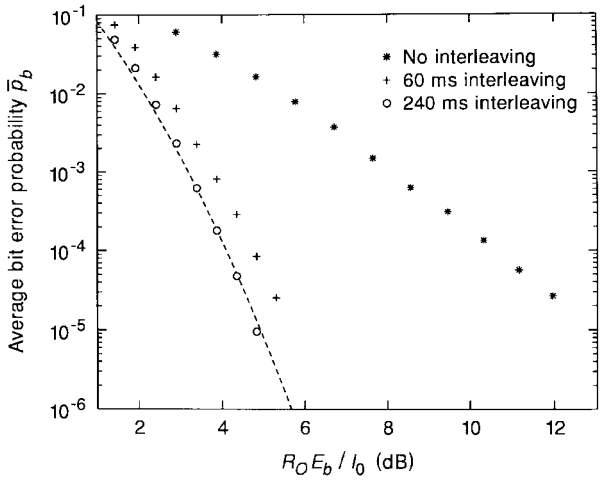

Fig. 6. Convolutional code performance for correlated Rayleigh fading four-path channels (vehicle speed 25 km/h, carrier frequency $f_0 = 2.232$ GHz).

TCH/D64. For the simulations, a Rayleigh fading multipath channel with $L' = 4$ equal-strength paths has been assumed. Furthermore, the correlation function of every path follows the popular Jakes Doppler model, which solely depends on the vehicle speed and the carrier frequency. In our simulations, these parameters were assumed to be 25 km/h and $f_0 = 2.232$ GHz (uplink), corresponding to a Doppler frequency of $f_D = 51.66$ Hz. In addition, an inner block interleaver, where data are read in row by row and read out column by column, and a four-branch Rake receiver utilizing ideal channel estimates have been used. Simulations were run for the cases of no inner interleaving, inner interleaving with a 60-ms delay (606 rows and 16 columns), and finally inner interleaving with a 240-ms delay (1212 rows and 32 columns). The latter interleaver size closely follows the practical rule of thumb: $0.4/(f_D T_s)$ rows and $5M$ columns. Increasing the interleaving delay even further did not yield any performance

TABLE I
PARAMETERS FOR CHANNEL CODING AND SPREADING ASSOCIATED WITH TCH/Dx AND DCCH

	TCH/D9.6 (NB)	TCH/D9.6 (MB)	TCH/D64 (MB)	TCH/D128 (MB)	DCCH (NB)	DCCH (MB)
Source rate	9.6 kbit/s	9.6 kbit/s	64 kbit/s	128 kbit/s	9.6 kbit/s	9.6 kbit/s
Outer code	RS(60,48,8)	RS(60,48,8)	RS(100,80,8)	RS(100,80,8)	RS(30,24,8)	RS(30,24,8)
Inner code rate R_I	1/2	1/2	1/2	1/2	1/2	1/2
Memory M	6	6	6	6	6	6
Channel rate $1/T_s$	24.8 kbit/s	24.8 kbit/s	161.6 kbit/s	323.2 kbit/s	24.8 kbit/s	24.8 kbit/s
Chip rate $1/T_c$	1.023 Mchip/s	5.115 Mchip/s	5.115 Mchip/s	5.115 Mchip/s	1.023 Mchip/s	5.115 Mchip/s
Spreading factor g	41	206	31	15	41	206

improvement. Thus, for all practical purposes, an interleaving delay of 240 ms represents ideal interleaving. The dashed line in Fig. 6 has been computed by using the first six terms of the series expansion of the bound in (18). Fig. 6 indicates the excellent agreement between the theoretical results and simulations. Furthermore, it demonstrates that for speeds $\geq$25 km/h, an inner interleaver with a 60-ms delay performs almost as well as an ideal interleaver does. Inner interleavers with a 60-ms delay have been selected for both TCH/D64 and TCH/D128.

The choice of the RS code parameters is dictated by the data rate, the 10-ms frame size, the maximum allowable total interleaving delay of 120 ms, and the outer interleaver depth. For TCH/D9.6, TCH/D64, and TCH/D128, these considerations resulted in an RS codeword span of 40 ms $(k_O = 48)$, 10 ms $(k_O = 80)$, and 5 ms $(k_O = 80)$, respectively. Having fixed k_O, the rate of the RS codes has been optimized [18] by applying the performance analysis presented in the preceding sections. Fig. 7 shows the probability of codeword error P_W as a function of the RS codeword length n_O for $k_O = 80$. The probability of codeword error P_W has been computed from (30) by using the first six terms of the series expansion of the symbol-error probability bound in (28) for the equal-strength Rayleigh fading multipath channel and a Rake receiver with $L = L'$ branches. Four cases have been considered: $L' = 1$ $(E_b/I_0 = 4.70$ dB), $L' = 2$ $(E_b/I_0 = 3.73$ dB), $L' = 3$ $(E_b/I_0 = 3.42$ dB), and $L' = 4$ $(E_b/I_0 = 3.26$ dB). The particular values of E_b/I_0 have been selected such that the achievable probability of codeword error is approximately 10^{-5}. Fig. 7 shows that there is an optimum RS code rate for a particular fading multipath channel. Clearly, for an operating point of $P_W \approx 10^{-5}$, an RS codeword length of $n_O = 100$, i.e., $R_O = 0.8$, is a very good choice for all fading multipath channels considered here. Similarly, it was found that for the same operating point and $k_O = 48$, an RS codeword length of $n_O = 60$, i.e., $R_O = 0.8$, is again a very good choice for all fading multipath channels considered here. Note that the optimum rate of the RS outer code depends on the number of paths (diversity) and the operating point of the inner convolutional code. For example, as the diversity increases, the optimum RS code rate becomes larger.

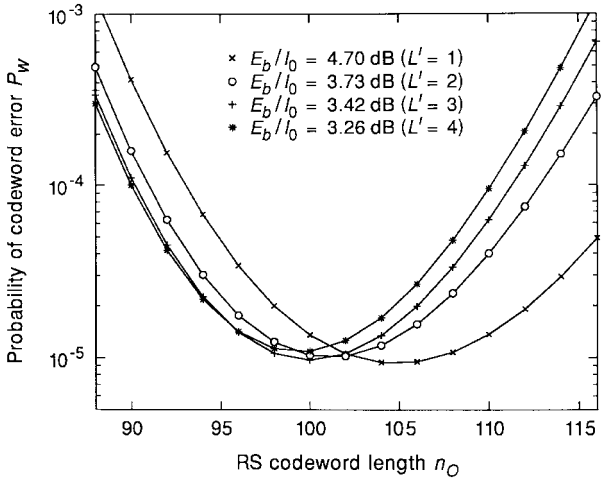

Fig. 7. Optimum RS code rate for $k_O = 80$.

Table I summarizes the parameters for channel coding and spreading associated with TCH/Dx and DCCH. Finally, Fig. 8 shows the performance of the concatenated coding scheme for TCH/D9.6 and TCH/D64 in terms of the probability of bit error P_b at the output of the RS decoder as a function of E_b/I_0. These results have been obtained from (31) by using the first six terms of the series expansion of the symbol-error probability bound in (28).

An estimate of the single-cell CDMA capacity [3] of the CODIT system can be derived from (3) by considering the auxiliary PCCH's as additional interfering users. Let E_c' be the chip energy associated with the auxiliary PCCH, and let E_c be the chip energy associated with the information-bearing PDCH for the uplink. Thus, for K simultaneous users in a cell, the bit energy to interference power spectral density ratio for the reference user is

$$\frac{E_b}{I_0} = \frac{(g/R)E_c}{\alpha E_c + \beta(K-1)E_c + \beta K E_c' + N_0}. \qquad (35)$$

For a channel with equal-strength paths and normalized energy equal to one, (A14) yields $\alpha = 1 - 1/L'$. Furthermore, for the square-root raised-cosine pulse-shaping filters used in the CODIT system, we have $\beta = 0.9125$ [see (B1)]. Neglecting the thermal noise contribution in (35) and taking

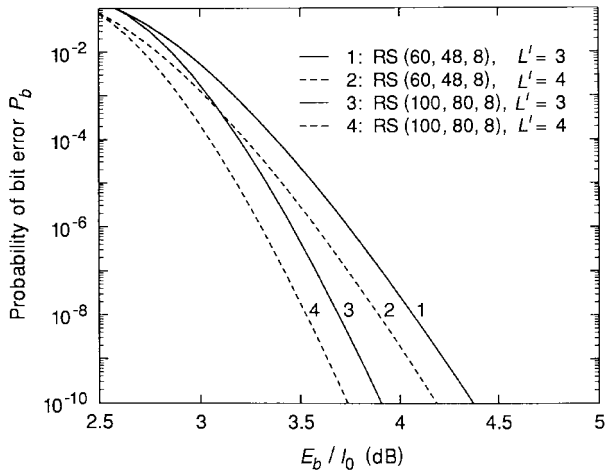

Fig. 8. Concatenated coding performance for equal-strength Rayleigh fading multipath channels.

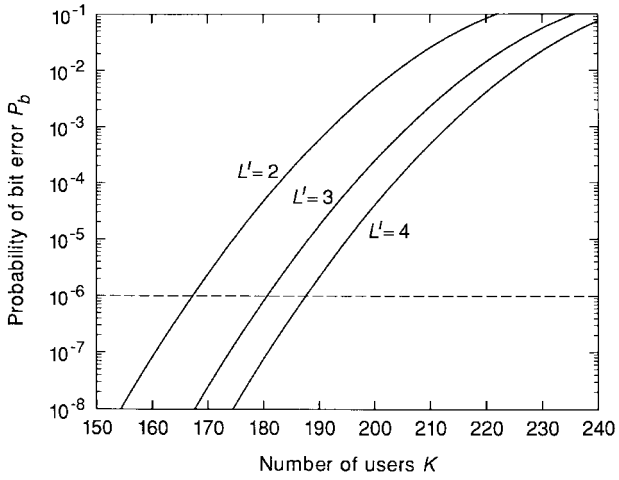

Fig. 9. Single-cell CDMA capacity of TCH/D9.6 in the medium band.

$\alpha+\beta(K-1) \approx \beta K$, the single-cell CDMA capacity becomes

$$K = \frac{g/R}{\beta[1+E_c'/E_c](E_b/I_0)}. \tag{36}$$

Fig. 9 shows the probability of bit error P_b as a function of the number of simultaneous users K in a single cell for 9.6-kbit/s data service in the medium band. The ratio $E_c'/E_c = -4.95$ dB has been optimized via computer simulations. For an operating point of $P_b = 10^{-6}$, it can be seen that a single cell can support $K = 166$, 180, and 187 simultaneous users for $L' = 2$, 3, and 4 paths, respectively. Clearly, Fig. 9 demonstrates the soft capacity of CDMA cellular systems, i.e., that the error rate performance of the system degrades gradually with an increasing number of users.

VI. Conclusions

A concatenated coding scheme employing inner convolutional codes and outer RS codes for reliable data transmission in DS–CDMA cellular systems has been proposed. A simple model for the memoryless inner coding channel of a DS–CDMA system that uses nonperiodic random spreading sequences and a coherent Rake receiver has been derived. This model, which treats multiple-access interference in a fading multipath environment, applies to systems that use time-limited or band-limited pulse shaping.

The performance of a DS–CDMA system employing RS/convolutional codes has been analyzed by using new, easy-to-compute upper bounds on the bit- and symbol-error probabilities of convolutional codes over Nakagami, Rayleigh, and Rician fading multipath channels. These bounds can be expressed in terms of the generating function of the convolutional codes, and are particularly tight for error rates less than 10^{-3}. Furthermore, the use of the convolutional code bounds in optimizing the rate of the RS outer code has been demonstrated.

The design of the RS/convolutional error control scheme of the data traffic and dedicated control channels in the CODIT system has been presented, and the tradeoffs between performance and maximum number of simultaneous users in a cell have been studied. The performance results indicate that the concatenated coding scheme based on inner convolutional codes and outer RS codes is a powerful approach for providing high data reliability in DS–CDMA cellular systems.

Appendix A
Equivalent Communications System Model

Let $\tilde{s}_1(i)$ in Fig. 1(a) denote the chip-spaced sequence of the reference user after inner interleaving and spreading of the BPSK modulated data sequence $x_1(n)$, i.e., $\tilde{s}_1(i) = \tilde{x}_1(\lfloor i/g \rfloor)s_1(i)$, where $|\tilde{s}_1(i)|^2 = E_c$ and E_c is the chip energy. Let also $p(t)$ denote the impulse response of the pulse-shaping filter where, without loss of generality, a unit energy filter is assumed. The received signal at the output of the equivalent end-to-end baseband channel of Fig. 1(b) [see (1)] can then be expressed as

$$\begin{aligned} r(t) = &\sum_{j=-\infty}^{\infty} \tilde{s}_1(j) \sum_{m=1}^{L'} h_{1m} p(t - jT_c - \tau_{1m}) \\ &+ \sum_{q=2}^{K} \sum_{j=-\infty}^{\infty} \tilde{s}_q(j) \sum_{m=1}^{L'} h_{qm} p(t - jT_c - \tau_{qm} - \Delta_q) \\ &+ \eta(t) \end{aligned} \tag{A1}$$

where Δ_q denotes the relative transmission delay of the qth user with respect to the first user (reference user) and h_{qm} stands for the complex amplitude of the mth path seen by the qth user. The dependency of h_{qm} on time has been neglected for notational simplicity. In (A1), the first term represents the signal received due to the first user, the second term denotes the multiple access interference due to the $K-1$ other users in the same cell (intracell interference), and the third term represents complex additive white Gaussian noise with variance N_0. After matched filtering and despreading, the received chip-spaced sequence at the input of the accumulator in the lth branch of the Rake receiver in Fig. 1(c) is

$$\nu_{1l}(i) = \nu_{1l}^{\text{signal}}(i) + \nu_{1l}^{\text{self}}(i) + \nu_{1l}^{\text{intra}} + \nu_{1l}^{\text{noise}}(i) \tag{A2}$$

where $\nu_{1l}^{\text{signal}}(i)$ denotes the desired chip-spaced signal received via the lth branch of the Rake receiver, $\nu_{1l}^{\text{self}}(i)$ is

the self-noise due to the reception of the desired signal via $L'-1$ other paths, $\nu_{1l}^{\text{intra}}(i)$ is the intracell interference, and $\nu_{1l}^{\text{noise}}(i)$ is the thermal noise. In the following, the path delay differences are assumed to be a multiple of T_c.

It can be shown that the desired signal is given by

$$\nu_{1l}^{\text{signal}}(i) = s_1^*(i)h_{1l}\sum_{j=-\infty}^{\infty} s_1(j)\tilde{x}_1(\lfloor j/g\rfloor)R_p((i-j)T_c) \tag{A3}$$

where $R_p(\cdot)$ is the autocorrelation function of the impulse response of the pulse-shaping filter $p(t)$. If $p(t)$ is a band-limited signal and $R_p(\cdot)$ satisfies the Nyquist criterion, then (A3) becomes

$$\nu_{1l}^{\text{signal}}(i) = h_{1l}\tilde{x}_1(\lfloor i/g\rfloor), \tag{A4}$$

i.e., interchip interference is eliminated. For example, this is the case for the family of square-root raised-cosine pulse-shaping filters. Clearly, (A4) is also valid for time-limited signals, i.e., $p(t), 0 \le t \le T_c$, such as the rectangular pulses prevalent in the spread-spectrum literature. The noise term in (A2) is given by

$$\nu_{1l}^{\text{noise}}(i) = s_1^*(i)\int_{-\infty}^{\infty} p(t)\eta(t+iT_c+\tau_{1l})\,dt. \tag{A5}$$

Similarly, the intracell interference term in (A2) can be expressed as

$$\begin{aligned}\nu_{1l}^{\text{intra}}(i) = {} & s_1^*(i)\sum_{q=2}^{K}\sum_{j=-\infty}^{\infty}\tilde{s}_q(j)\sum_{m=1}^{L'}h_{qm} \\ & \cdot R_p((i-j)T_c+\tau_{1l}-\tau_{qm}-\Delta_q)\end{aligned} \tag{A6}$$

where $\tilde{s}_q(i)$ denotes the chip-spaced transmitted sequence of the qth user after BPSK modulation, inner interleaving, and spreading, and $|\tilde{s}_q(i)|^2 = E_c$. Finally, the self-noise due to the reception of the desired signal via $L'-1$ other paths can be expressed by

$$\begin{aligned}\nu_{1l}^{\text{self}}(i) = {} & s_1^*(i)\sum_{j=-\infty}^{\infty}\tilde{s}_1(j)\sum_{\substack{m=1\\ m\neq l}}^{L'}h_{1m} \\ & \cdot R_p((i-j)T_c+\tau_{1l}-\tau_{1m}).\end{aligned} \tag{A7}$$

Let $w_{1l}(n)$ be the symbol-spaced signal at the output of the accumulator on the lth Rake branch, i.e.,

$$w_{1l}(n) = \sum_{i=ng}^{(n+1)g-1}\nu_{1l}(i). \tag{A8}$$

Furthermore, let $w_{1l}^{\text{signal}}(n), w_{1l}^{\text{self}}(n), w_{1l}^{\text{intra}}(n)$, and $w_{1l}^{\text{noise}}(n)$ denote the four components of $w_{1l}(n)$ representing the desired signal, the self-noise, the intracell interference, and the thermal noise, respectively.

Following the approach used in [8], we condition the various interference terms at the output of the accumulator on the spreading sequence of the reference user $s_1(i)$ and compute their conditional variances. It can readily be seen that $w_{1l}^{\text{noise}}(n)$ is a sequence of independent Gaussian random variables with zero mean and conditional variance given by

$$\mathrm{E}[|w_{1l}^{\text{noise}}(n)|^2] = gR_p(0)N_0 = gN_0. \tag{A9}$$

Proceeding similarly, the conditional variance of the intracell interference can be expressed by

$$\begin{aligned}&\mathrm{E}[|w_{1l}^{\text{intra}}(n)|^2] \\ &\quad = E_c\sum_{q=2}^{K}\sum_{m=1}^{L'}\mathrm{E}[|h_{qm}|^2]\sum_{i_1=ng}^{(n+1)g-1}\sum_{i_2=ng}^{(n+1)g-1}s_1^*(i_1) \\ &\qquad \cdot s_1(i_2)\phi((i_1-i_2)T_c) \\ &\quad = \phi(0)gE_c\sum_{q=2}^{K}\sum_{m=1}^{L'}\mathrm{E}[|h_{qm}|^2]\Bigg(1+\frac{1}{\phi(0)g} \\ &\qquad \cdot \sum_{i_1=ng}^{(n+1)g-1}\sum_{\substack{i_2=ng\\ i_2\neq i_1}}^{(n+1)g-1}s_1^*(i_1)s_1(i_2)\phi((i_1-i_2)T_c)\Bigg)\end{aligned} \tag{A10}$$

where the expectation on the left-hand side is taken with respect to the random spreading sequences, the channel statistics, and the relative transmission delays Δ_q (uniformly distributed over the interval $[0,T_c)$) of the $K-1$ other users and

$$\begin{aligned}\phi(\tau) \equiv {} & \mathrm{E}\left[\sum_{j=-\infty}^{\infty}R_p(jT_c+\tau-\Delta_q)R_p(jT_c-\Delta_q)\right] \\ = {} & \frac{1}{T_c}\int_{-\infty}^{\infty}R_p(t)R_p(t+\tau)\,dt.\end{aligned} \tag{A11}$$

Arguing similarly as in [8], the second term in the parentheses in (A10) can be expressed as a weighted sum of partial autocorrelations of the random spreading sequence and can therefore be neglected. Alternatively, viewing the conditional variance in (A10) as a random variable, the second term in the parentheses has zero mean and variance that is upper bounded by $(2/g)\ \Sigma_{i=1}^{+\infty}\ \phi^2(iT_c)/\phi^2(0)$. By using the Poisson sum formula, this upper bound can be shown to be finite for time-limited or band-limited pulses $p(t)$. Furthermore, as it can be made as small as desired by selecting the processing gain g sufficiently large, (A10) can be approximated by

$$\mathrm{E}[|w_{1l}^{\text{intra}}(n)|^2] = \beta gE_c\sum_{q=2}^{K}\sum_{m=1}^{L'}\mathrm{E}[|h_{qm}|^2] \tag{A12}$$

where $\beta \equiv \phi(0)$. Note that (A12) becomes exact for brick-wall pulse-shaping filters with bandwidth $1/T_c$. For AWGN channels, (A12) simplifies to $\mathrm{E}[|w_{1l}^{\text{intra}}(n)|^2] = \beta(K-1)gE_c$, as derived in [12] and [24]. In Appendix B, β has been computed for widely used pulse-shaping filters, and it is shown that under a unit energy constraint, β satisfies the inequality $0 < \beta \le 1$.

The analysis of self-interference is more complicated, and its small contribution to the total interference for large K is either ignored [7] or included as an additional user [8]. Proceeding similarly as above, we approximate the conditional variance of the self-interference by its mean or equivalently treat self-interference as an additional chip-synchronized interfering user over a channel with $L'-1$ paths, i.e.,

$$\mathrm{E}[|w_{1l}^{\text{self}}(n)|^2] = gE_c\sum_{\substack{m=1\\ m\neq l}}^{L'}\mathrm{E}[|h_{1m}|^2] \le \alpha gE_c \tag{A13}$$

where

$$\alpha \equiv \left(\sum_{m=1}^{L'} \mathrm{E}[|h_{1m}|^2] - \min_{1 \le m \le L} \mathrm{E}[|h_{1m}|^2] \right). \tag{A14}$$

For large g, arguing as above, we assume that self-interference and thermal noise on different Rake branches are uncorrelated. Similarly, for the correlation of multiple-access interference, we obtain

$$\mathrm{E}[w_{1l_1}^{\mathrm{intra}}(n)(w_{1l_2}^{\mathrm{intra}}(n))^*] = \phi(\tau_{1l_1} - \tau_{1l_2}) g E_c \sum_{q=2}^{K} \sum_{m=1}^{L'} \mathrm{E}[|h_{qm}|^2] \tag{A15}$$

where $1 \le l_1, l_2 \le L$. Equation (A15) indicates that the intracell interference on different branches of the Rake receiver is generally correlated. For square-root raised-cosine pulse-shaping filters with rolloff parameter $0 \le \varrho \le 1$, a closed-form expression for $\phi(\tau_{1l_1} - \tau_{1l_2})$ can be obtained:

$$\phi(rT_c) = \begin{cases} 1 - \varrho/4, & \text{if } r = 0 \\ \dfrac{(-1)^{r+1} \sin(\pi \varrho r)}{4\pi r(1 - \varrho^2 r^2)}, & \text{if } r \neq 0 \end{cases} \tag{A16}$$

where $r = (\tau_{1l_1} - \tau_{1l_2})/T_c$ is an integer. Clearly, the intracell interference on different branches of the Rake receiver is uncorrelated, i.e., $\phi(rT_c) = 0$ for $r \neq 0$, only in the case of a brickwall filter ($\varrho = 0$). Similarly, for rectangular pulse shaping, (A11) yields

$$\phi(rT_c) = \begin{cases} 2/3, & \text{if } r = 0 \\ 1/6, & \text{if } r = \pm 1 \\ 0, & \text{otherwise.} \end{cases} \tag{A17}$$

Equations (A16) and (A17) suggest that the uncorrelatedness of the intracell interference on different branches of the Rake receiver (see also [8]) generally is a good approximation. In particular, this approximation is extremely good for square-root raised-cosine filters with small values of ϱ, which is the case in most practical CDMA systems.

Using the approximation of uncorrelated intracell interference, thermal noise, and self-interference, it can be seen that, conditioned on the data symbol $\tilde{x}_1(n)$ and the complex amplitudes $h_{1l}, 1 \le l \le L$, the mean and the variance of the signal $\tilde{y}_1(n)$ at the deinterleaver input are given by

$$\mathrm{E}[\tilde{y}_1(n)] = g\tilde{x}_1(n) \sum_{l=1}^{L} |h_{1l}|^2 \tag{A18}$$

$$\begin{aligned} \mathrm{var}\,[\tilde{y}_1(n)] &= \frac{g}{2} \sum_{l=1}^{L} |h_{1l}|^2 \,\mathrm{var}\,[w_{1l}^{\mathrm{self}}(n) + w_{1l}^{\mathrm{intra}}(n) + w_{1l}^{\mathrm{noise}}(n)] \\ &= g \sum_{l=1}^{L} |h_{1l}|^2 \left(\frac{E_c}{2} \sum_{\substack{m=1 \\ m \neq l}}^{L'} \mathrm{E}[|h_{1m}|^2] + \frac{E_c}{2}\beta \cdot \sum_{q=2}^{K} \sum_{m=1}^{L'} \mathrm{E}[|h_{qm}|^2] + \frac{N_0}{2} \right). \end{aligned} \tag{A19}$$

Thus, using (A18), the tight bound of (A13) in (A19), and the Gaussian approximation for large K [8], we arrive at the simple communications system model depicted in Fig. 2. In this model, the total interference is represented by the additive zero mean white Gaussian interference source $N(0, I_0/2)$, whose variance is given by

$$\frac{I_0}{2} = \frac{E_c}{2}\alpha + \frac{E_c}{2}\beta \sum_{q=2}^{K} \sum_{m=1}^{L'} \mathrm{E}[|h_{qm}|^2] + \frac{N_0}{2} \tag{A20}$$

and the effects of multipath fading and of coherent Rake reception are characterized by two identical multiplicative random variables preceding and following the total interference source. From one symbol interval to the next, these random variables are independent, owing to ideal inner interleaving/deinterleaving. The preceding analysis has demonstrated that the model in Fig. 2 is a good approximation of the overall system shown in Fig. 1, and hence this model is referred to as the equivalent communications system model.

Appendix B
On the Pulse-Shaping Coefficient β

Assuming typical unit energy pulse-shaping filters, one obtains from (A11) for $\tau = 0$

$$\beta \equiv \phi(0) = \begin{cases} 2/3, & \text{if } p(t) \text{ is rectangular} \\ 1, & \text{if } p(t) \text{ is sinc function} \\ 1 - \varrho/4, & \text{if } p(t) \text{ is square-root raised-cosine.} \end{cases} \tag{B1}$$

The case of rectangular pulses resulting in $\beta = 2/3$ was first obtained in [25], whereas the case of brickwall pulse-shaping filters resulting in $\beta = 1$ is presented in [12] and [24].

For pulses that are either time-limited to an interval of length T_c or band-limited such that their autocorrelation function satisfies the Nyquist criterion, we have $R_p(nT_c) = \delta(n)$ or, equivalently,

$$\sum_{i=-\infty}^{\infty} \left| P\left(f - \frac{i}{T_c}\right) \right|^2 = T_c, \qquad -\infty \le f \le \infty. \tag{B2}$$

Equation (B2) implies

$$|P(f)|^2 \le T_c, \qquad -\infty \le f \le \infty. \tag{B3}$$

Hence, using Parseval's relation in (A11) for $\tau = 0$, (B3) and the unit energy constraint for the pulse-shaping filter, we obtain

$$\beta = \frac{1}{T_c} \int_{-\infty}^{\infty} |P(f)|^4 \, df \le \frac{1}{T_c} \int_{-\infty}^{\infty} |P(f)|^2 T_c \, df = 1. \tag{B4}$$

Thus,

$$0 < \beta \le 1. \tag{B5}$$

Note that a lower bound $\beta \ge 1/(WT_c)$ has been obtained in [12] and [24] assuming pulse-shaping filters that are strictly band-limited to bandwidth W. Clearly, the upper bound in (B5) and the lower bound in [12] and [24] become equal, i.e., $\beta = 1$, for brickwall filters with bandwidth $W = 1/T_c$. Finally, it is worth noting that β is also used in a different context to define a quantity known as the mitigation bandwidth $W_m = 2/(\beta T_c)$ [9]. For the class of pulse-shaping filters considered here, the

bound in (B5) translates into a lower bound on the mitigation bandwidth, i.e., $W_m \geq 2/T_c$.

ACKNOWLEDGMENT

The authors would like to thank their colleagues in the project CODIT for fruitful cooperation, and the reviewers for their valuable comments.

REFERENCES

[1] A. Baier, U.-C. Fiebig, W. Granzow, W. Koch, P. Teder, and J. Thielecke, "Design study for a CDMA-based third-generation mobile radio system," *IEEE J. Select. Areas Commun.*, vol. 12, pp. 733–743, May 1994.

[2] P.-G. Andermo and L.-M. Ewerbring, "A CDMA-based radio access design for UMTS," *IEEE Personal Commun.*, vol. 2, no. 1, pp. 48–53, 1995.

[3] K. S. Gilhousen, I. M. Jacobs, R. Padovani, A. J. Viterbi, L. A. Weaver, and C. E. Wheatley, "On the capacity of a cellular CDMA system," *IEEE Trans. Veh. Technol*., vol. 40, pp. 303–312, May 1991.

[4] R. D. Cideciyan and E. Eleftheriou, "Performance of concatenated coding scheme for data transmission in CDMA cellular systems," in *Proc. RACE Mobile Telecommun. Workshop*, Metz, France, June 1993. pp. 465–469.

[5] ———, "Concatenated coding scheme for reliable data transmission in CDMA cellular systems," presented at the Int'l Zurich Seminar Digital Commun.; also, in *Lecture Notes in Computer Science*, vol. 783, C. Günther, Ed. Berlin, Heidelberg: Springer-Verlag, 1994, pp. 76–86.

[6] R. Price and P. E. Green, "A communication technique for multipath channels," *Proc. IRE*, vol. 46, pp. 555–578, Mar. 1958.

[7] J. Wang and L. B. Milstein, "CDMA overlay situations for microcellular mobile communications," *IEEE Trans. Commun.*, vol. 43, pp. 603–614, Feb./Mar./Apr. 1995.

[8] T. Eng and L. B. Milstein, "Coherent DS-CDMA performance in Nakagami multipath fading," *IEEE Trans. Commun.*, vol. 43, pp. 1134–1143, Feb./Mar./Apr. 1995.

[9] F. Amoroso, "Use of DS/SS signaling to mitigate Rayleigh fading in a dense scatterer environment," *IEEE Personal Commun. Mag*, vol. 3, no. 2, pp. 52–61, 1996.

[10] S. Y. Mui and J. W. Modestino, "Comparison of convolutional and block code performance on the Rician channel," in *Proc. IEEE Nat. Telecommun. Conf.*, 1977, pp. 20:4-1–20:4-7.

[11] J. Hagenauer, "Viterbi decoding of convolutional codes for fading- and burst-channels," in *Proc. Int. Zurich Seminar*, Zurich, Switzerland, Mar. 1980, pp. G2.1–G2.7.

[12] A. J. Viterbi, *CDMA: Principles of Spread Spectrum Communication*. Reading, MA: Addison-Wesley, 1995.

[13] M. B. Pursley and D. J. Taipale, "Error probabilities for spread-spectrum packet radio with convolutional codes and Viterbi decoding," *IEEE Trans. Commun.*, vol. COM-35, pp. 1–12, Jan. 1987.

[14] R. K. Morrow and J. S. Lehnert, "Packet throughput in slotted ALOHA DS/SSMA radio systems with random signature sequences," *IEEE Trans. Commun.*, vol. 40, pp. 1223–1230, July 1992.

[15] B. D. Woerner and W. E. Stark, "Improved upper bounds on the packet error probability of slotted and unslotted DS/SS systems," *IEEE Trans. Commun.*, vol. 43, pp. 3055–3062, Dec. 1995.

[16] A. J. Viterbi and J. K. Omura, *Principles of Digital Communication and Coding*. New York: McGraw-Hill, 1979.

[17] M. Nakagami, "The m-distribution—A general formula of intensity distribution of rapid fading," in *Statistical Methods in Radio Wave Propagation*, W. G. Hoffman, Ed. Oxford, U.K.: Pergamon, 1960, pp. 3–36.

[18] R. D. Cideciyan and E. Eleftheriou, "Concatenated Reed–Solomon/convolutional coding scheme for data transmission in CDMA cellular systems," in *Proc. IEEE Veh. Technol. Conf.*, Stockholm, Sweden, June 1994, pp. 1369–1373.

[19] M. Abramowitz and I. A. Stegun, Eds., *Handbook of Mathematical Functions*, Appl. Math. Ser., vol. 55. Washington, DC: Nat. Bur. Stand., 1972.

[20] R. D. Cideciyan and E. Eleftheriou, "New bounds on convolutional code performance over fading channels," in *Proc. IEEE Int. Symp. Inform. Theory*, Trondheim, Norway, July 1994, p. 270.

[21] R. J. McEliece and I. M. Onyszchuk, "A symbol error upper bound for convolutional codes," in *Proc. 27th Allerton Conf.*, Monticello, IL, Sept. 1989, pp. 334–335.

[22] I. M. Onyszchuk, "Finding the complete path and weight enumerators of convolutional codes," TDA Progress Rep., JPL, pp. 203–213, Feb. 1990.

[23] J. P. Odenwalder, "Error control coding handbook," Final Rep. under Contract F44620-76-C-0056 for USAF, Linkabit Corp., July 1976.

[24] A. J. Viterbi, "Very low rate convolutional codes for maximum theoretical performance of spread-spectrum multiple-access channels," *IEEE J. Select. Areas Commun.*, vol. 8, pp. 641–649, May 1990.

[25] M. B. Pursley, "Performance evaluation for phase-coded spread-spectrum multiple access communication—Part I: System analysis," *IEEE Trans. Commun.*, vol. COM-25, pp. 795–799, Aug. 1977.

Roy D. Cideciyan (S'82–M'86) was born in Istanbul, Turkey, on August 7, 1956. He received the Dipl.-Ing. degree from Aachen University of Technology (RWTH), Aachen, Germany, in 1981 and the M.S.E.E. and Ph.D. degrees from the University of Southern California, Los Angeles, in 1982 and 1985, respectively.

He joined the IBM Research Division, Zurich Research Laboratory, Rüschlikon, Switzerland, in 1986, where he has been working in the areas of signal processing and coding for magnetic recording, coding for Gbit/s local-area networking, and wireless transmission. In 1995, he served as the Editor of the final report on the radio interface of the CODIT project. His research interests include signal processing, synchronization and coding for data transmission, and magnetic recording.

Evangelos Eleftheriou (S'81–M'86) was born in Aliveri, Euboea, Greece, on February 15, 1955. He received the degree in electrical engineering from the University of Patras, Greece, in 1979, and the M.Eng. and Ph.D. degrees from Carleton University, Ottawa, Canada, in 1981 and 1985, respectively.

He joined the IBM Zurich Research Laboratory, Rüschlikon, Switzerland, in 1986, where he has been working on high-speed voiceband data modems, wireless communications, and coding and signal processing for magnetic recording channels. His research interests include digital communications, signal processing, and coding.

Since January 1994, Dr. Eleftheriou has served as Editor for Equalization and Coding of IEEE TRANSACTIONS ON COMMUNICATIONS.

Marcel Rupf was born in 1961 and grew up in Rorschach, Switzerland. He received the M.S. and Ph.D. degrees in electrical engineering from the Swiss Federal Institute of Technology (ETH), Zurich, Switzerland, in 1987 and 1993, respectively.

From 1993 to 1995, he did his Post Doctorate at the IBM Zurich Research Laboratory, Rüschlikon, Switzerland. At present, he is with Siemens Schweiz AG, Zurich, where he is involved in mobile communications projects.